Optical Cherenkov radiation in ultrafast cascaded second-harmonic generation

Citation: Bache, M. et al. "Optical Cherenkov Radiation in Ultrafast Cascaded Second-harmonic Generation." Physical Review A 82.6 (2010) : 063806. © 2010 The American Physical Society

As Published: http://dx.doi.org/10.1103/PhysRevA.82.063806

Publisher: American Physical Society

Persistent URL: http://hdl.handle.net/1721.1/62842

Version: Final published version: final published article, as it appeared in a journal, conference proceedings, or other formally published context

Optical Cherenkov radiation in ultrafast cascaded second-harmonic generation

M. Bache,[1,*] O. Bang,[1] B. B. Zhou,[1] J. Moses,[2] and F. W. Wise[3]

[1]*DTU Fotonik, Department of Photonics Engineering, Technical University of Denmark, DK-2800 Kgs. Lyngby, Denmark*

[2]*Optics and Quantum Electronics Group, Massachusetts Institute of Technology, Cambridge, Massachusetts 02139, USA*

[3]*Department of Applied and Engineering Physics, Cornell University, Ithaca, New York 14853, USA*

(Received 5 October 2010; published 3 December 2010)

We show through theory and numerics that when few-cycle femtosecond solitons are generated through cascaded (phase-mismatched) second-harmonic generation, these broadband solitons can emit optical Cherenkov radiation in the form of linear dispersive waves located in the red part of the spectrum. The beating between the dispersive wave and the soliton generates trailing temporal oscillations on the compressed soliton. Insertion of a simple short-wave pass filter after the crystal can restore a clean soliton. On the other hand, bandpass filtering around the dispersive wave peak results in near-transform-limited ultrashort mid-IR pulses with pulse durations much shorter than the input near-IR pulse. The Cherenkov radiation for the crystal considered (β-barium borate) is found for pump wavelengths in the range $\lambda = 0.95$–1.45 μm, and is located in the regime $\lambda = 1.5$–3.5 μm. For shorter pump wavelengths, the phase-matching point is located in the absorption region of the crystal, effectively absorbing the generated dispersive wave. By calculating the phase-matching curves for typically used frequency conversion crystals, we point out that the mid-IR absorption in the crystal in many cases automatically will filter away the dispersive wave. Finally, an investigation of recent experimental results uncovers a four-wave-mixing phenomenon related to Cherenkov radiation that is an additional generation mechanism of long-wavelength radiation that can occur during soliton compression. We discuss the conditions that lead to this alternative dynamics rather than generation of Cherenkov radiation.

DOI: 10.1103/PhysRevA.82.063806 PACS number(s): 42.65.Tg, 42.65.Re, 42.65.Ky, 42.65.Sf

I. INTRODUCTION

One of the most celebrated and investigated nonlinear processes is second-harmonic generation (SHG) [1]. Despite this fact, there are today still new aspects to discover, in particular when ultrafast pulses in the femtosecond regime interact. We here discuss optical Cherenkov radiation through radiation of linear dispersive waves [2] when ultrashort few-cycle solitons are generated through cascaded SHG.

Cascaded SHG occurs when the nonlinear conversion process over the propagation length L is strongly phase mismatched $|\Delta kL| \gg 1$: up-conversion to the second harmonic (SH) is followed by the reverse process of down-conversion to the fundamental wave (FW) after half a coherence length $\pi/2|\Delta k|$. On continued propagation, the SH is therefore cyclically generated and back-converted (the cascade of nonlinear effects). In this cascaded nonlinear interaction the FW experiences a nonlinear phase shift due to the difference in phase velocities, and the magnitude and sign of the phase shift are determined by the phase-mismatch parameter Δk [3]. This property is useful for many applications (see Ref. [4] for a review).

One particular application is pulse compression of energetic femtosecond pulses toward the few-cycle regime with cascaded quadratic nonlinearities [5,6]. In this particular example a strong negative nonlinear phase shift is generated on the FW by the cascaded nonlinearity, which means that, unlike in many other media, solitons may now be excited even in regimes with normal dispersion (where blue components travel more slowly than red components). An important regime is the visible and near-IR, in which soliton compression of femtosecond pulses is possible even to few-cycle duration [7]. Furthermore, the cascaded nonlinearity can be understood as a Kerr-like self-phase-modulation (SPM) action, and the negative sign of this effective nonlinearity means that it is self-defocusing. Thus, catastrophic collapse due to self-focusing effects may be avoided provided that the self-focusing material Kerr nonlinearities can be overcome [8], and it is therefore possible to compress multiple millijoule femtosecond pulses with this method. Therefore this method is a compact and efficient alternative to existing compression methods, such as, e.g., pulse compression in hollow fibers combined with dispersive elements [9], for generating energetic few-cycle pulses.

Recently we investigated how close to the ultimate limit (single-cycle duration $T = 2\pi/\omega$) this soliton compression system can get [10]. In this connection we noted that higher-order dispersion (HOD) in the numerics revealed surprising features of the compressed soliton, namely, a peak in the nonsolitonic part of the spectrum, and we suggested that it could be optical Cherenkov radiation. This peak disappeared when only up to third-order dispersion was used. We will here investigate this phenomenon in detail.

The first prediction of resonant dispersive waves came from Wai *et al.*, who showed that when perturbing the nonlinear Schrödinger equation (NLSE) with HOD, e.g., third-order dispersion, the otherwise stable soliton will start to radiate energy into a dispersive wave [2,11]. This was later coined optical "Cherenkov" radiation, since the soliton propagates through the medium emitting radiation with a slower group velocity [12]. The first experimental observation of optical Cherenkov radiation came shortly after in a mode-locked dye laser generating solitonlike pulses [13] and in a single-mode fiber [14]; both systems are well described by the NLSE. A similar effect called Kelly sidebands [15] can be observed in soliton fiber lasers, where periodical gain may induce nonsolitonic radiation in the sidebands of the laser spectrum.

*moba@fotonik.dtu.dk

The dispersive wave is linear in nature and feeds off the generated solitons in the system, and its spectral location is a result of a phase-matching condition to the soliton [12]. Dispersive waves are often found in supercontinuum generation outside the soliton regions [16,17], where solitons are no longer supported because the group-velocity dispersion (GVD) changes sign (see [18] for a review). Currently there is also focus on use of dispersive waves for ultrashort pulse synthesis [19] and broadband frequency combs [20].

In this publication we investigate the presence of dispersive waves in cascaded SHG of ultrafast femtosecond pulses. We derive the nonlocal NLSE governing the FW, and show that in the stationary regime and weakly nonlocal limit, a description of the FW dynamics by a standard NLSE with HOD is well justified. We derive the phase-matching conditions for the dispersive wave as a function of the FW soliton wavelength, and calculate specifically the conditions for a standard nonlinear crystal. These calculations show that a dispersive wave can form on the red side of the spectrum (at longer wavelengths), and it is clear that including only a few extra orders of dispersion is often not enough to describe the dispersive wave formation accurately as the dispersive wave may be strongly redshifted from the soliton. Through numerical simulations we investigate the formation of the dispersive waves in detail, and show that the theoretical predictions are quite accurate. We show how the dispersive wave can be removed after the soliton is formed by using a simple short-wave pass filter after the nonlinear crystal. On the other hand, the dispersive wave radiation can also be isolated with a bandpass filter, resulting in an ultrashort near-transform-limited mid-IR pulse. We calculate the phase-matching curves for a broad range of standard frequency conversion crystals, and point out that in the more dispersive crystals the phase-matching condition is often found inside the absorption region of the crystal. Finally, we discuss some experimental results obtained by some of us in connection with another study [21] in order to understand whether the spectral peaks, which were observed in the linear (anomalous) regime, are related to optical Cherenkov radiation. This investigation helps us to differentiate between two closely related mechanisms for the generation of long-wavelength radiation that can occur during cascaded-quadratic soliton compression.

II. THEORY

Consider the propagation equations for SHG in mks units. In a type-I phase-matching configuration two degenerate FW photons with frequency ω_1 combine to give a SH photon $\omega_2 = 2\omega_1$ with orthogonal polarization with respect to the FW. In the slowly-varying-envelope approximation and in absence of diffraction the governing propagation equations for the electric fields E_j are [22,23]

$$\left[i\frac{\partial}{\partial z} + \hat{D}_1\right]E_1 + \frac{\omega_1 d_{\text{eff}}}{cn_1}E_1^* E_2 e^{i\Delta k z} = 0, \tag{1}$$

$$\left[i\frac{\partial}{\partial z} - id_{12}\frac{\partial}{\partial \tau} + \hat{D}_2\right]E_2 + \frac{\omega_1 d_{\text{eff}}}{cn_2}E_1^2 e^{-i\Delta k z} = 0, \tag{2}$$

where d_{eff} is the effective $\chi^{(2)}$ nonlinearity. Later in the numerical simulations we will extend these equations to the slowly-evolving-wave approximation [7,23] and include also competing Kerr nonlinearities and self-steepening effects. The equations have been transformed to the frame of reference traveling with the FW group velocity $v_{g,1} = 1/k_1^{(1)}$ by the retarded time coordinate $\tau = t - z/v_{g,1}$, which gives rise to the group-velocity mismatch (GVM) term $d_{12} = k_1^{(1)} - k_2^{(1)}$. The phase mismatch is $\Delta k = k_2 - 2k_1$, and the equations are generalized to include dispersion up to order m_d through the operators $\hat{D}_j = \sum_{m=2}^{m_d} \frac{i^m}{m!} k_j^{(m)} \frac{\partial^m}{\partial \tau^m}$, and $k_j^{(m)} \equiv d^m k_j / d\omega^m|_{\omega=\omega_j}$ are the dispersion coefficients, $k_j = n_j\omega/c$ the wave numbers, and n_j the linear refractive indices, whose chromatic dispersion is modeled by the Sellmeier equations [24].

A. NLSE describing cascaded SHG

We consider strongly phase-mismatched (cascaded) SHG, in which the FW can be approximately described by a NLSE [22]. More precisely, we recently showed [10,25] that in the cascading limit $|\Delta k|z \gg 1$, the ansatz $E_2(z,\tau) = \phi(\tau)e^{-i\Delta k z}$ when inserted in Eq. (2) and Fourier transformed, yields the solution in the frequency domain

$$\tilde{E}_2(z,\Omega) = -e^{-i\Delta k z}\sqrt{2\pi}\frac{\omega_1 d_{\text{eff}}}{cn_2\Delta k}\tilde{R}(\Omega)\mathcal{F}\left[E_1^2(z,\tau)\right], \tag{3}$$

where $\mathcal{F}[\cdot]$ denotes the forward Fourier transform. The nonlocal response function in the frequency domain, $\tilde{R}$, is

$$\tilde{R}(\Omega) = \frac{1}{\sqrt{2\pi}}\frac{\Delta k}{\hat{D}_2(\Omega) - d_{12}\Omega + \Delta k}, \tag{4}$$

where $\hat{D}_2(\Omega) = \sum_{m=2}^{m_d} m!^{-1} k_2^{(m)} \Omega^m$ is the SH dispersion operator in the Fourier domain. Using the convolution theorem $E_2(z,\tau) = -e^{-i\Delta k z}\frac{\omega_1 d_{\text{eff}}}{cn_2\Delta k}\int_{-\infty}^{\infty} ds R(s) E_1^2(z,\tau - s)$, where $R(\tau) = \mathcal{F}^{-1}[\tilde{R}]$ is the inverse Fourier transform of the response function. Inserting this into Eq. (1) and normalizing the variables, we see that the FW obeys a dimensionless nonlocal NLSE,

$$\left[i\frac{\partial}{\partial \xi} + \hat{D}_1'\right]U_1 + N_{\text{Kerr}}^2 U_1|U_1|^2 - \text{sgn}(\Delta k)N_{\text{SHG}}^2 U_1^* \int_{-\infty}^{\infty} ds R'(s) U_1^2(\xi, \tau' - s) = 0. \tag{5}$$

Here $\tau' = \tau/T_{\text{in}}$, where T_{in} is the FW input pulse duration, $\xi = z/L_{\text{D},1}$, where $L_{\text{D},1} = T_{\text{in}}^2/|k_1^{(2)}|$ is the FW dispersion length, and finally $U_1 = E_1/\mathcal{E}_{\text{in}}$ with $\mathcal{E}_{\text{in}}$ being the peak amplitude of the electric input field. The dimensionless dispersion is $\hat{D}_j' = \sum_{m=2}^{m_d} i^m \delta_j^{(m)} \frac{\partial^m}{\partial \tau'^m}$ and $\delta_j^{(m)} \equiv k_j^{(m)}(T_{\text{in}}^{m-2}|k_1^{(2)}|m!)^{-1}$.

The dimensionless nonlocal response function $R'(\tau') = T_{\text{in}}R(\tau)$ determines the nature of the cascaded SHG interaction, and in most cases (see also below) it results in an instantaneous and a delayed Kerr-like SPM term. This part is controlled by the cascaded soliton order

$$N_{\text{SHG}}^2 = L_{\text{D},1}\mathcal{E}_{\text{in}}^2\frac{\omega_1^2 d_{\text{eff}}^2}{c^2 n_1 n_2 |\Delta k|}. \tag{6}$$

In Eq. (5) we have also included Kerr SPM in the material (but we neglect for simplicity cross-phase-modulation effects as they remain weak because the SH is inefficiently converted). The Kerr soliton order is $N_{\text{Kerr}}^2 = L_{\text{D},1}\frac{\omega_1}{c} I_{\text{in}} n_{\text{Kerr}}^I$, where the Kerr nonlinear refractive index is $n_{\text{Kerr}}^I = \frac{3\text{Re}(\chi_{\text{eff}}^{(3)})}{4\varepsilon_0 n_1^2 c}$, with I_{in} as

the FW peak input intensity and $\chi^{(3)}_{\rm eff}$ the appropriate cubic nonlinear tensor component of the interaction (see Ref. [26] for more details).

In the so-called stationary regime, where the cascaded nonlinear effects dominate GVM effects, the denominator of Eq. (4) has only complex roots in Ω, making the nonlocal response function $|R| \propto e^{-|\tau|/\tau_s}$. In the stationary regime the weakly nonlocal approximation is often satisfied [10], in which the response function is much narrower than the pulse width $\tau_s \ll T_{\rm in}$, and the NLSE can be approximated as [10,25]

$$\left[i\frac{\partial}{\partial\xi} + \hat{D}_1'\right] U_1 - \left[\mathrm{sgn}(\Delta k) N_{\rm SHG}^2 - N_{\rm Kerr}^2\right] U_1 |U_1|^2 = \mathrm{sgn}\left(\Delta k d_{12} k_2^{(2)}\right) i N_{\rm SHG}^2 \tau_{R,\rm SHG} |U_1|^2 \frac{\partial U_1}{\partial\tau}. \quad (7)$$

From this equation the left-hand side tells us that in the cascading limit the FW experiences an overall cubic nonlinearity. For $\Delta k > 0$ the cascaded SHG contribution is negative, i.e., self-defocusing, and we may in this case introduce an effective soliton order $N_{\rm eff}^2 = N_{\rm SHG}^2 - N_{\rm Kerr}^2$ to describe the effective nonlinear strength. In the normal dispersion regime $\delta_j^{(2)} > 0$, a FW soliton may then be induced by the cascaded SHG if $\Delta k > 0$. This ensures an overall effective self-defocusing cubic nonlinearity. We can also interpret the effective cubic nonlinearity through an intensity-dependent change in the refractive index $n = n_1 + I_1 n^I_{\rm cubic}$, where $n^I_{\rm cubic} = n^I_{\rm SHG} + n^I_{\rm Kerr}$. From our analysis the contribution from the cascaded quadratic nonlinearities is $n^I_{\rm SHG} = -\frac{2\omega_1 d_{\rm eff}^2}{c^2\varepsilon_0 n_1^2 n_2 \Delta k}$, consistent with Ref. [3], and we have in the self-defocusing case $N_{\rm eff}^2 = L_{\rm D,1}\frac{\omega_1}{c} I_{\rm in} |n^I_{\rm cubic}| = L_{\rm D,1}\frac{\omega_1}{c} I_{\rm in}(|n^I_{\rm SHG}| - n^I_{\rm Kerr})$. The requirement of an overall effective self-defocusing cubic nonlinearity then comes down to having $|n^I_{\rm SHG}| > n^I_{\rm Kerr}$.

The right-hand side of Eq. (7) represents the weakly nonlocal contribution of the cascaded nonlinearity. It is a self-steepening-like term that, in combination with the nonlinear phase shifts from the stationary component of the nonlinear polarization, produces a Raman-like frequency shift that tends to blueshift the soliton for $\mathrm{sgn}(\Delta k d_{12} k_2^{(2)}) < 0$ (as is the case with normal dispersion and self-defocusing effective nonlinearity). It is governed by a characteristic dimensionless time parameter $\tau_{R,\rm SHG} = 2|d_{12}/T_{\rm in}\Delta k|$. Thus, the blueshift is small for long input pulses and for $N_{\rm SHG}$ small. Evidently a strong GVM in the interaction will also affect this term, as will a reduced phase mismatch Δk. However, when we stay in the stationary regime the characteristic time $\tau_{R,\rm SHG}$ remains small and the blueshift remains insignificant. This is further justified if $N_{\rm SHG}$ is not too large since the nonlocal self-steepening-like term is proportional to $N_{\rm SHG}^2$; see Eq. (7). The stationary regime is the parameter space for which $\Delta k > \Delta k_{\rm sr}$, where $\Delta k_{\rm sr} = d_{12}^2/2k_2^{(2)}$ is the phase-mismatch parameter, at which the roots of the denominator in Eq. (4) change from being complex to being real for $m_d = 2$ [25]. If $\Delta k < \Delta k_{\rm sr}$ (the nonstationary regime), GVM effects become very strong, and the interaction can no longer be described as simply as the right-hand side of Eq. (7); see Ref. [10] for more details. The blueshift is described in more detail in Ref. [27]; note that this study operated with a low Δk (and was thereby conducted in the nonstationary regime) where the blue-shift is much stronger since $\tau_{R,\rm SHG}$ increases.

In the rest of this section we therefore base our calculations on the following NLSE:

$$\left[i\frac{\partial}{\partial\xi} + \hat{D}_1'\right] U_1 - N_{\rm eff}^2 U_1 |U_1|^2 = 0. \quad (8)$$

We will now proceed to calculate the phase-matching conditions for optical Cherenkov radiation.

B. Optical Cherenkov radiation

When only second-order dispersion (GVD) is considered we get the standard NLSE

$$\left[i\frac{\partial}{\partial\xi} - \delta_1^{(2)}\frac{\partial^2}{\partial\tau^2}\right] u_1 - u_1|u_1|^2 = 0, \quad (9)$$

where $\delta_1^{(2)} = \mathrm{sgn}(k_1^{(2)})/2 = 1/2$ in the case of normal dispersion, and where $u_1 = U_1 N_{\rm eff}$. It has the following soliton solution [12]:

$$u^0_{1,\rm sol} = A\ \mathrm{sech}(A\tau) e^{i q'_{\rm sol}\xi}, \quad (10)$$

where A is the peak amplitude of the soliton and insertion of Eq. (10) into Eq. (9) yields the dimensionless soliton wave number $q'_{\rm sol} = -A^2/2$. The negative sign is due to the fact that we are dealing with self-defocusing nonlinearities.

In order to observe optical Cherenkov radiation, it is not enough to consider the NLSE with only GVD (9); we must include some perturbation in the form of HOD. Basically HOD tends to destabilize the stable soliton solution (10): the soliton can become phase matched to a linear wave, which extracts energy from the soliton. We can find this phase-matching point by requiring that the phase of the soliton be that of the dispersive wave $\phi_{\rm sol} = \phi_{\rm dw}$. The phase accumulated by the soliton at a propagation distance L is $\phi_{\rm sol} = L[n_1(\omega_{\rm sol})\omega_{\rm sol}/c + q_{\rm sol} - \omega_{\rm sol}/v_{g,\rm sol}]$, where $v_{g,\rm sol} = 1/k_1^{(1)}(\omega_{\rm sol})$ is the group velocity at the soliton frequency. Using the result from before and converting to physical units we get $q_{\rm sol} = -N_{\rm eff}^2 I_{\rm sol}/(2L_{\rm D,1} I_{\rm in}) = -|n^I_{\rm cubic}| I_{\rm sol}\omega_1/2c$, where $I_{\rm sol}$ is the peak intensity of the soliton.

This is identical with the expression in Ref. [16] except for the sign of the nonlinear term. The dispersive wave must in order to be efficiently generated move in the same reference frame as the pump, but since it is a linear wave it will not contain any nonlinear phase shift. Its phase is therefore simply $\phi_{\rm dw} = L[n_1(\omega_{\rm dw})\omega_{\rm dw}/c - \omega_{\rm dw}/v_{g,\rm sol}]$. Phase-matching $\phi_{\rm sol} = \phi_{\rm dw}$ therefore implies

$$\frac{n_1(\omega_{\rm dw})\omega_{\rm dw} - n_1(\omega_{\rm sol})\omega_{\rm sol}}{c} - \frac{\omega_{\rm dw} - \omega_{\rm sol}}{v_{g,\rm sol}} - q_{\rm sol} = 0. \quad (11)$$

At this point one could simply just start finding the frequency $\omega_{\rm dw}$ that fulfills this requirement for a given $\omega_{\rm sol}$. However, in the stationary reference frame we may equivalently state the following identity for the soliton wave number including nonlinear corrections [28]:

$$k_{\rm sol}(\omega) = k_1(\omega_{\rm sol}) + (\omega - \omega_{\rm sol})k_1^{(1)}(\omega_{\rm sol}) + q_{\rm sol}. \quad (12)$$

The solitonic (nondispersive) nature is evident through the linear dependence on ω of the soliton wave number. The phase-matching condition can now be written as

$k_1(\omega_{dw}) - k_{sol}(\omega_{dw}) = 0$, i.e., at the dispersive wave frequency the soliton and the linear dispersive wave have the same wave number. Expanding the wave number of the linear radiation $k_1(\omega_{dw})$ around ω_{sol}, this condition may be expressed as

$$\sum_{m=2}^{m_d} \frac{(\omega_{dw} - \omega_{sol})^m}{m!} k_1^{(m)}(\omega_{sol}) - q_{sol} = 0 \qquad (13)$$

with $m_d = \infty$. The sum is now recognized as the FW dispersion operator expanded around the soliton frequency, evaluated at the frequency ω_{dw}, and taking into account all orders of dispersion. Clearly, this phase-matching condition is sensitive to how many orders of dispersion are included in the analysis. Obviously, this is especially the case if the soliton is far from the zero-dispersion point.

In order to evaluate the phase-matching condition we need to know the soliton peak intensity I_{sol}, and a valid estimate can be found by using the scaling laws for cascaded SHG [23]. Specifically, the peak soliton intensity at the optimal compression point can be estimated by $I_{sol} = f_c Q_c I_{in}$, where the compression factor is $f_c = 4.7(N_{eff} - 0.86)$ and the compressed pulse quality is $Q_c = [1 + 0.24(N_{eff} - 1)^{1.11}]^{-1}$. It is at this point convenient for our case to use this result to write the soliton wave number as $q_{sol} = -N_{eff}^2 f_c Q_c / 2L_{D,1}$, giving

$$q_{sol} = -\frac{|k_1^{(2)}| N_{eff}^2 4.7(N_{eff} - 0.86)}{2T_{in}^2[1 + 0.24(N_{eff} - 1)^{1.11}]}. \qquad (14)$$

For a fixed N_{eff} and input pulse duration T_{in} the only wavelength-dependent term is the GVD coefficient $k_1^{(2)}$.

These analytical results will now be tested against numerical simulations presented in the next section.

III. NUMERICAL SIMULATIONS

In our recent work [10] we observed an unexpected spectral peak in the mid-IR when simulating cascaded SHG pulse compression in β–barium borate (BBO) for type-I phase-matching pumping with $\lambda_1 = 1.064\ \mu$m and including all orders of dispersion. However, when only up to third-order dispersion ($m_d = 3$) was included, the peak disappeared. We argued that this peak was a dispersive wave phase matched to the soliton, and in order to investigate this further, we have here carried out simulations at other wavelengths.[1]

Before showing the numerical results, it is instructive to mention the rather peculiar dispersion conditions we operate with. Dispersive waves have mainly been studied in Kerr systems with a self-focusing nonlinearity where solitons

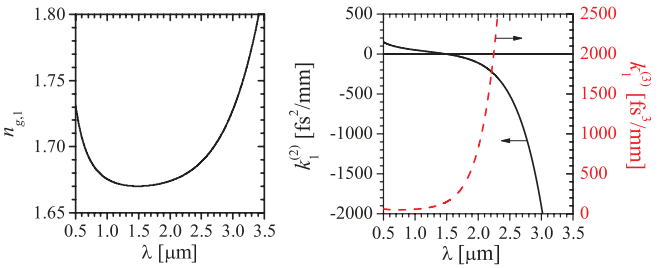

FIG. 1. (Color online) The wavelength dependence of (a) the FW group index $n_{g,1} = c/v_{g,1}$; (b) FW GVD $k_1^{(2)}$ (black) and FW TOD $k_1^{(3)}$ (red, dashed) for BBO.

are generated in the anomalous dispersion regime. In our system the effective nonlinearity is, as mentioned before, self-defocusing, and solitons therefore reside in the normal dispersion regime. The FW group index, GVD, and third-order dispersion (TOD) coefficients for BBO are shown in Fig. 1.The normal dispersion regime is for $\lambda < \lambda_{ZD} \simeq 1.49\ \mu$m, and the dispersion slope is positive.

The numerical results are summarized in Fig. 2, and the main simulation parameters are listed in Table I. Generally, dispersive waves are observed for a range of soliton wavelengths spanning the zero-dispersion wavelength λ_{ZD} down to around $\lambda_1 = 0.95\ \mu$m. Below this wavelength the dispersive wave becomes phase matched in the mid-IR absorption band of BBO ($\lambda > 3.5\ \mu$m) and can therefore no longer be observed. In the figure we also present the results of the theory:[2] the dashed thin black line is the phase-matching condition Eq. (13) taking into account the nonlinear correction to the soliton phase via Eq. (14), while the solid thick black line neglects this contribution (i.e., takes $q_{sol} = 0$). We deliberately used a short pulse [50 fs full width at half maximum (FWHM)] and a moderate effective soliton order[3] ($N_{eff} = 2.0$) in order to simplify the temporal and spectral dynamics; due to the rather short input pulse duration, for higher soliton orders the compressed solitons became more distorted, making it harder to determine precisely the location of the dispersive wave. Another justification for keeping low soliton orders is that the simple NLSE (8) is also more accurate for small values of the soliton order N_{SHG}. By keeping a low effective soliton order, the nonlinear correction to the phase-matching condition is kept small; there is a clear but small deviation only close to λ_{ZD}.

Commenting briefly on our result from Ref. [10], we observed that there a dispersive wave when pumping with $\lambda_1 = 1.064\ \mu$m and using exact dispersion, while it disappeared with only TOD. In Fig. 2 it is clear from the phase-matching curve for TOD ($m_d = 3$, red dotted curve) that around

[1]The simulations are based on the full coupled SHG propagation equations in the slowly-evolving-wave approximation [21] (see [23] for more details), and they include exact dispersion ($m_d = \infty$), self-steepening, and Kerr effects. We do not model a noninstantaneous Kerr (Raman) response because the ultrafast Raman response function for BBO is to our knowledge not known. For more details, see Ref. [23], but note that we have in the present publication used a larger Kerr nonlinearity, $n_{Kerr}^I = 5.9 \times 10^{-20}$ m^2/W, based on observations made in Ref. [21], and the IR-corrected Sellmeier equations [24]. We use Miller's rule to determine the chromatic dispersion of the nonlinear coefficients (see [26] for more details).

[2]In order to calculate the phase-matching curves we used the Sellmeier equations for BBO with IR corrections [24]: these should be valid all the way up to $\lambda \simeq 3.2\ \mu$m. This is important in order to calculate the dispersion correctly. See also the discussion later in connection with Fig. 6.

[3]Note that an effective soliton order of 2.0 may seem quite low, but the input pulse being as short as 50 fs FWHM the scaling laws for the cascaded soliton compression [23] predict a sub-10 fs FWHM compressed soliton, which for the wavelengths considered here corresponds to as little as two or three optical cycles.

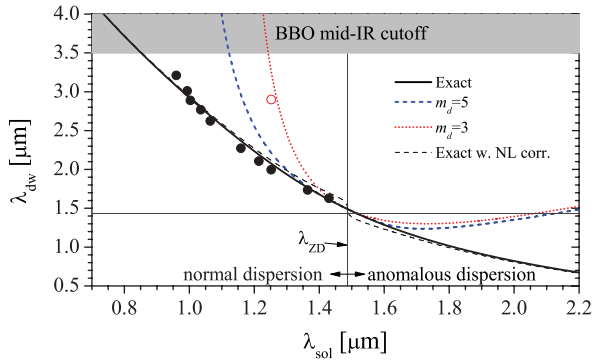

FIG. 2. (Color online) Summary of numerical simulations of cascaded pulse compression in BBO cut for type-I ($oo \rightarrow e$) phase matching at various FW wavelengths. The filled black circles show the numerically observed Cherenkov radiation wavelength peak at the propagation distance where the FW soliton is compressed to its shortest duration ($z = z_{opt}$). The data are plotted as a function of the soliton wavelength λ_{sol} as determined by a cross-correlation frequency-resolved optical gating spectrogram (see, e.g., Fig. 4 later). The theoretical phase-matching curves are calculated from Eq. (13), and the thick curves are taking $q_{sol} = 0$ and using $m_d = 3$ (red, dotted), $m_d = 5$ (blue, dashed) or exact dispersion (black), while the thin dashed black curve is for exact dispersion and k_{sol} from Eq. (14). This curve is possible to calculate since $N_{eff} = 2.0$ and $T_{in} = 28.4$ fs are held fixed. All simulations are done with exact dispersion except for one using only TOD (red, open circle). For other parameters, see Table I.

$\lambda_1 = 1.06\ \mu$m the phase-matching point λ_{dw} for $m_d = 3$ is far into the mid-IR absorption band, and thus the dispersive wave will be absorbed; we were therefore not able to observe it in our study in Ref. [10]. This is also the case when including up to fifth-order dispersion (blue dashed curve). Only with higher-order dispersion (in this case exact, or all orders, of dispersion) is the dispersive wave accurately described. This is because the pump wavelength is so far away from the zero-GVD point. When pumping with a longer wavelength close to the zero-GVD point, the TOD case can show a dispersive wave, and we confirmed this with a simulation for $\lambda_1 = 1.300\ \mu$m (red open circle), which matches the theory quite well.

The dispersive wave is seen to form to the red side of the spectrum, because the nonsolitonic regime due to the effective self-defocusing nonlinearity resides in the anomalous dispersion region. In contrast, in silica fibers dispersive waves are typically observed in the blue part of the spectrum. This is because the nonlinearity in fibers is self-focusing, implying that solitons require anomalous GVD to exist, and the linear regime (normal dispersion) is located to the blue side. On the other hand, redshifted dispersive waves have also been observed with self-focusing nonlinearities: it was initially suggested [29] and subsequently experimentally demonstrated [30] that redshifted dispersive waves may extend the continuum further into the infrared. This was achieved by using photonic crystal fibers with very small cores that made it possible to get two zero-dispersion points, one to the blue and one to the red side of the soliton. Such a dispersion profile has been used to study, e.g., soliton self-frequency shift cancellation [31] and to generate broadband IR radiation using a near-IR pump [32].

While the phase-matching condition might allow a dispersive wave to form independently on the soliton spectral bandwidth, it is only when there is a spectral overlap between the soliton spectrum and the Cherenkov resonance that it grows to a substantial level [33]. Therefore Cherenkov radiation is usually observed when the soliton is formed close to λ_{ZD}. However, in the case we have considered here the solitons were compressed to few-cycle duration through the cascaded interaction, and their spectra were therefore ultrabroadband. This is the reason why we could observe Cherenkov radiation very far away from the soliton wavelength.

The detailed dynamics in the creation of the ultrashort FW soliton and subsequently the dispersive wave can be appreciated in Fig. 3, which shows a simulation at $\lambda_1 = 1.300\ \mu$m with exact dispersion. In the simulation the 50 fs input pulse is after around 32 mm of propagation compressed to a 12 fs FWHM (sub-three-cycle) soliton; see Fig. 3(a). This compression occurs due to the cascaded SHG; the SHG coherence length for the chosen phase-mismatch parameter $\Delta k = 20\ \text{mm}^{-1}$ is very short, $L_{coh} = \pi/|\Delta k| = 0.16$ mm, and thus hundreds of cascaded conversion cycles have occurred at the optimal compression point. At the compression point the FW soliton shows trailing oscillations, and subsequently radiation is emitted at a slower group velocity than the soliton: this is optical Cherenkov radiation. Eventually the soliton detaches from the uncompressed pedestal, which at the end of the simulation ($z = 100$ mm) is located on the leading side around $\tau = -20$ fs.

In the FW spectrum, Fig. 3(c), the soliton is blueshifted due to the nonlocal terms that induce a Raman-like frequency shift. A careful investigation shows that the soliton at the compression point is located around $\lambda = 1.25\ \mu$m, and at this propagation stage resonant Cherenkov radiation appears,

TABLE I. Parameters of the simulations used in Fig. 2. The phase mismatch is continuously changed to satisfy $\Delta k > \Delta k_{sr}$, and at the same time low enough to achieve $|n^I_{SHG}| > n^I_{Kerr}$. The characteristic time parameter of the nonlocal self-steepening-like term in Eq. (7) is kept roughly constant, $\tau_{R,SHG} \simeq 0.11$–0.16, for all simulations. Input parameters: $N_{eff} = 2.0$, sech-shaped pulse with $T_{in}^{FWHM} = 50$ fs ($T_{in} = 28.4$ fs), which ideally should generate a sub-10 fs FWHM compressed soliton [23]. The dispersion is calculated from the Sellmeier equations in Ref. [24].

λ_1 (μm)	Δk (mm^{-1})	Δk_{sr} (mm^{-1})	I_{in} (GW/cm^2)	N_{SHG}	N_{Kerr}	λ_{dw} (μm)	z_{opt} (mm)
0.950	80	79	1319	8.7	8.5	3.212	29
1.000	70	61	474	5.6	5.2	3.011	25
1.030	60	52	229	4.2	3.7	2.888	17
1.064	55	43	176	3.8	3.3	2.769	17
1.100	45	36	101	3.2	2.5	2.624	17
1.200	30	19	43	2.7	1.8	2.273	22
1.260	30	15	40	2.8	1.9	2.108	28
1.300	20	10	19	2.4	1.4	1.998	32
1.400	20	5.1	11	2.5	1.5	1.736	66
1.450	10	2.2	2.2	2.2	0.94	1.631	152

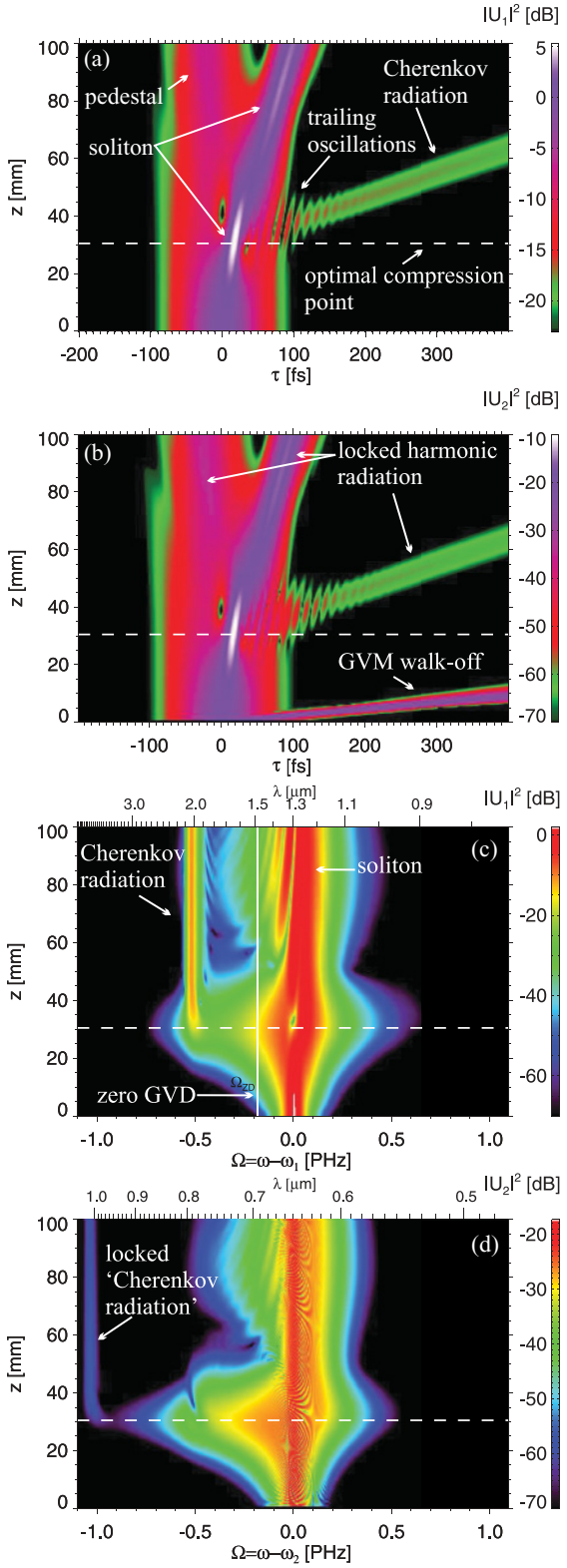

FIG. 3. (Color online) The simulation for $\lambda_1 = 1.300\ \mu$m with exact dispersion: The FW time trace (a) shows a soliton that compresses to 12 fs FWHM at $z = z_{opt} = 32$ mm (optimal compression point, dashed line). At this point the FW spectrum (c) shows resonant Cherenkov radiation emitted with a spectral peak at $\Omega_{dw} \simeq -0.5$ PHz. The SH time plot (b) and spectrum (d) show similar dynamics due to the harmonic locking of the SH field in the cascading limit.

located to the red side of the spectrum. No Cherenkov radiation is observed before this point because the soliton is not formed yet. At the observed soliton wavelength the theory predicts a dispersive wave located at $\lambda = 2.12\ \mu$m ($\Omega = -0.56$ PHz), which slightly overestimates the dispersive wave peak position in the spectrum located around $\lambda_{dw} = 2.00\ \mu$m ($\Omega_{dw} = -0.51$ PHz). This trend seems quite general for most of the simulations, as summarized in Fig. 2.

After the optimal compression point, the dispersive wave remains stable at the same wavelength. However, it was recently shown that in the NLSE radiation trapping of the soliton and the dispersive wave can under certain circumstances continuously shift the dispersive wave away from the zero-GVD point [34,35]. In our case this would mean a continuous shift of the dispersive wave peak toward longer wavelengths, and this does not happen. The explanation is as follows: The main dispersive radiation occurs when the soliton is compressed to its minimum duration because here the soliton has its highest peak intensity and its broadest spectrum. As the soliton and dispersive wave propagate further the dispersive wave peak in the FW spectrum, Fig. 3(c), remains fixed. This is because the dispersive wave is emitted at a wavelength having a much slower group velocity than the soliton (see Fig. 1). This group-velocity mismatch between the soliton and the dispersive wave is also quite evident in the time trace in Fig. 3(a). The soliton is temporally delayed due to the blueshift induced by the cascaded nonlocal nonlinearity, pushing the soliton toward lower wavelengths and thereby lower group velocity (see again Fig. 1). However, it never becomes slow enough to catch up with the dispersive wave, and therefore collision and subsequent trapping as described by Refs. [34,35] cannot occur.

In supercontinuum generation with anomalous dispersion, the Raman effect redshifts the soliton and thereby slows it down. This is in fact the driving force behind much of the dynamics involved in the generation of the broad spectrum, in particular of the spectral part generated by trapping the soliton and the dispersive wave through a Raman-mediated slowing down of the soliton. In our results presented here we have neglected the effect of a Raman-delayed Kerr nonlinearity in the simulations, since the Raman response of the crystal we simulated, BBO, is not well known. If we were to take Kerr Raman effects into account in the simulations, then this would not lead to radiation trapping either: the Raman effect would redshift the soliton, but because we operate in the normal dispersion regime this would actually speed up the soliton, making the group-velocity mismatch between the soliton and the dispersive wave even greater. On the other hand, a Raman-like frequency shift is intrinsic in the cascaded SHG interaction [25,27], and it would be very interesting to study the competition and dynamics between these two similar nonlinear processes. This would require detailed and accurate measurements of the SHG nonlinear crystals in order to determine the instantaneous material Kerr nonlinearity and the delayed ultrafast Raman response, such as the technique used in Ref. [36].

The SH also shows some interesting features. In particular the spectrum Fig. 3(d) has what appears to be a dispersive wave around $\Omega = -1.0$ PHz. However, this spectral component is actually just the FW dispersive wave picked up at twice the

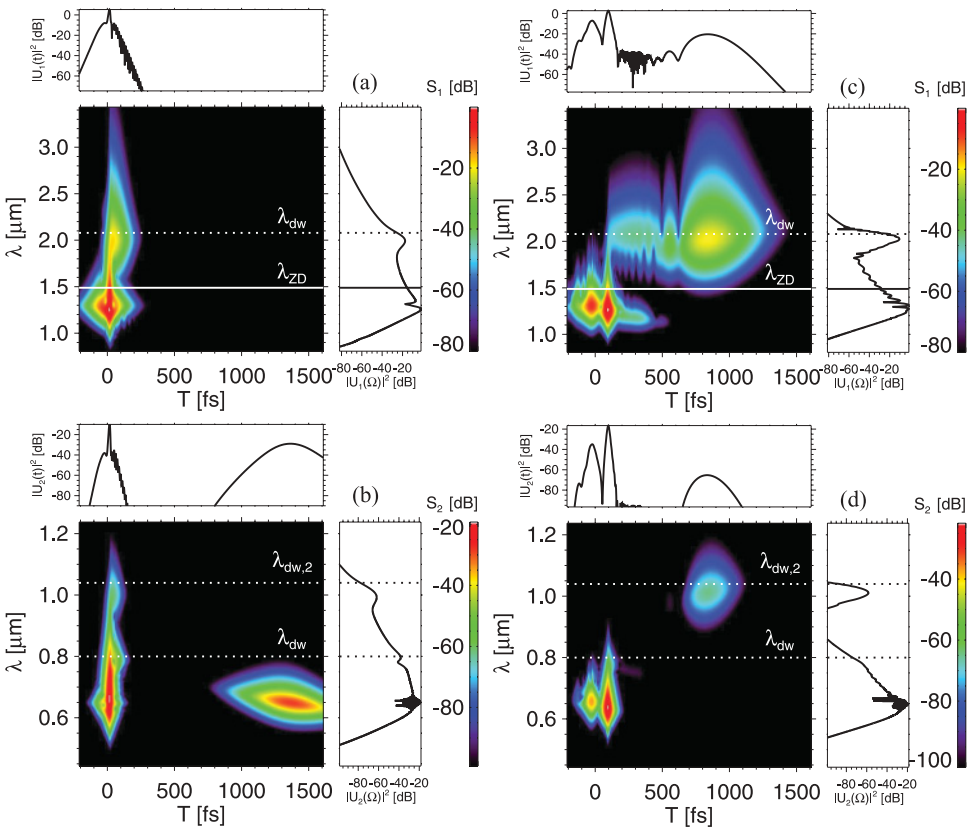

FIG. 4. (Color online) XFROG spectrograms of the FW (a), (c) and SH pulse (b), (d), taken at the optimal compression point $z = z_{\mathrm{opt}} = 32$ mm (left column) and at $z = 100$ mm (right column) for the simulation with $\lambda_1 = 1.300\ \mu$m and full dispersion. The dashed line λ_{dw} indicates the Cherenkov phase-matching point with the soliton at $\lambda_{\mathrm{sol}} = 1.25\ \mu$m. In the SH plots the lines $\lambda_{\mathrm{dw},2}$ indicate the wavelength beating with twice the predicted Cherenkov phase-matching frequency (see text). A sech-shaped gating pulse of 20 fs FWHM was used.

beat frequency $2\Omega_{\mathrm{dw}}$. This happens because in the cascading limit the SH spectrum is *locked* to the FW; cf. Eq. (3). This connection is modulated only by the nonlocal response function $\tilde{R}(\Omega)$. In the stationary regime $\Delta k > \Delta k_{\mathrm{sr}}$, where the simulations are carried out, and in the weakly nonlocal limit $\tilde{E}_2(z,\Omega) \simeq [\tilde{R}(\Omega = 0) + \Omega \frac{d\tilde{R}}{d\Omega}|_{\Omega=0}]\mathcal{F}[E_1^2(z,\tau)]$ [10]; thus the SH contains many of the same spectral components as the FW, and since it is locked to $\mathcal{F}[E_1^2(z,\tau)]$ it will contain frequency components at twice the frequency observed in the FW spectrum.

This locked "Cherenkov radiation" is also observable in the temporal trace of the SH; see Fig. 3(b). Note that it is traveling with the same group velocity as the FW dispersive wave, despite the fact that the SH group velocity at that wavelength ($\lambda \simeq 1.0\ \mu$m) is substantially lower. The GVM walk-off component of the SH is also observable: it appears in the beginning of the propagation as a rapidly disappearing term (due to a slower SH group velocity giving a substantial GVM parameter $d_{12} = -45$ fs/mm). Finally, the nonlocal locking of the SH to the FW also implies that the FW soliton and pedestal are "copied" in the SH time trace as locked harmonic radiation trapped in the frame of reference traveling with the FW group velocity. In another presentation we will investigate this phenomenon more closely [37].

While the harmonic locking effect evidently leaves distinct traces in the SH that are reminiscent of solitonic behavior, there is no proof that the locked SH radiation is actually a soliton. Therefore we do not believe that the locked radiation can generate resonant optical Cherenkov radiation. On the other hand, if we could observe Cherenkov radiation emitted by the SH, it would indicate that the SH was indeed a soliton, but the phase-matching point would be too far away in the spectrum to be observable.

A more detailed insight into optical Cherenkov radiation formation is obtained in Fig. 4, where the numerical results at $\lambda_1 = 1.300\ \mu$m are presented at the optimal compression point through cross-correlation frequency-resolved optical gating (XFROG) spectrograms, calculated as $S_j(\Omega,T) = \left|\int_{-\infty}^{\infty} d\tau' e^{i\Omega\tau'} U_j(\tau') U_{\mathrm{gate}}(\tau' - T)\right|^2$, where U_{gate} is a suitably chosen gating pulse. The FW in Fig. 4(a) has compressed to 12 fs FWHM and during compression it has been blueshifted to $\lambda_{\mathrm{sol}} = 1.25\ \mu$m. In the spectral trace as well as in the spectrogram the dispersive wave is quite evident: its position at $\lambda = 2.00\ \mu$m lies slightly below the wavelength predicted by the theory $\lambda_{\mathrm{dw}} = 2.12\ \mu$m for the observed soliton wavelength. On the logarithmic FW time trace on the top of Fig. 4(a) the trailing oscillations mentioned before are noticeable. These trailing oscillations have been studied analytically in detail in the NLSE including third-order dispersion [38]. From the spectrogram we can now explain them as a result of beatings between the linear dispersive wave and the soliton: in fact the temporal period (around 12 fs) is exactly the beat period $2\pi/|\Omega_{\mathrm{sol}} - \Omega_{\mathrm{dw}}|$. As the pulse propagates further through the crystal, the main part of the dispersive wave is delayed due to having a lower group velocity than the soliton [38], but at the same time new energy is fed into the dispersive wave. This position will now shift toward lower wavelengths after the optimal compression point; this is caused by a slight redshift toward a fixed final value of the soliton after the compression. This soliton redshift might be some kind of spectral recoil from losing energy to the dispersive wave, and eventually the saturation point could be due to a balance between the blueshift

induced by the nonlocal cascaded nonlinearity and the spectral recoil. A similar effect was observed in silica photonic crystal fibers with a negative dispersion slope in Ref. [31], where the Raman self-frequency shift is balanced by the blue recoil of the soliton losing energy to the dispersive wave.

In the spectrogram we also observe that upon propagation the amount of radiation shed into the dispersive wave region will diminish, mainly because soliton fission will occur, reducing the soliton intensity [39]. Another factor is that the dispersive wave strength is proportional to the spectral overlap of the soliton [33]. Thus, when the soliton is the shortest the radiation into the dispersive wave is strongest, and this occurs at the optimal compression point. Note that the total spectral intensity of the dispersive peak will instead grow upon propagation. This is because what is observed there is the sum of all the temporal slices of radiation shed by the soliton(s).

It is also worth noting that in Fig. 3(a) it seems that dispersive waves are emitted only at the optimal compression point, but actually weaker radiation is emitted subsequently by the soliton in the later relaxation stage, which is below the minimum level of the chosen color scale of that time trace. Instead in Fig. 4(c) it is evident that dispersive waves are continuously radiated by the soliton upon further propagation.

The SH spectrogram in Fig. 4(b) has two components: one locked to the FW pulse due to the cascaded interaction [cf. Eq. (3)], and one being the usual GVM walk-off component located around $T = +1300$ fs due to the lower group velocity. The beating of these two components causes the ripples in the SH spectrum around the degenerate SH wavelength $\lambda = 0.650\ \mu$m. The SH component created by the nonlocal locking to the FW at twice the dispersive wave frequency is quite obvious, indicated with $\lambda_{\mathrm{dw},2} = 2\pi c/(\omega_2 + 2\Omega_{\mathrm{dw}})$. In the time trace ripples similar to those of the FW are observed in the trailing part, but they oscillate faster as the beating frequency is twice that of the FW. Note also that the SH spectral cut actually has a hole where the FW dispersive wave resides.

We have also in Figs. 4(c) and 4(d) included the spectrograms taken upon further propagation ($z = 100$ mm). The FW now has a more "ragged" dispersive wave spectral cut, extending over a larger bandwidth than in the previous spectrum in Fig. 4(a). This is because, as mentioned above, the soliton after the compression point starts to redshift slightly, ending up at a wavelength slightly to the blue side of the original pump wavelength, and thus the phase-matching point shifts toward shorter wavelengths as the soliton propagates, giving a broader spectral peak.

In the SH spectrogram of Fig. 4(d) we observe the same features as at the previous propagation point: the locked harmonic travels with the FW group velocity and "copies" the FW radiation, while the FW dispersive wave components also leave signs in the SH spectrogram around $\lambda_{\mathrm{dw},2}$. In this spectrogram the SH GVM walk-off component is no longer inside the window shown (it appears at $T \simeq +4$ ps).

In a soliton compression context, the trailing temporal oscillations induced by optical Cherenkov radiation may not be desirable when striving for clean few-cycle pulses. However, they can easily be filtered away; see Figs. 5(a) and 5(b). This simulation is done for similar conditions as those used in the recent experiment by some of us [7]. From a 110 fs input pulse, a 9 fs FWHM compressed soliton is formed after 38 mm of propagation. The temporal trace is shown in Fig. 5(b) and the trailing oscillations due to the formation of Cherenkov radiation are quite pronounced (full black line). The dispersive wave is now filtered away by applying a short-wave pass filter centered slightly to the blue of the dispersive wave peak. The filtered soliton (dashed red line) has now a very clean shape without trailing oscillations and keeps a very short duration (11 fs FWHM). Thus, from a practical viewpoint this should not affect the generation of clean compressed solitons as long as the dispersive wave is generated substantially far away from the soliton wavelength.

On the other hand, the Cherenkov radiation may also act as a source of femtosecond IR radiation. In fact, if in the example discussed above we instead apply a suitable bandpass filter centered around the peak of the dispersive wave we can recover a $\lambda \simeq 2.11\ \mu$m pulse [see Fig. 5(c)], which has 50 fs FWHM

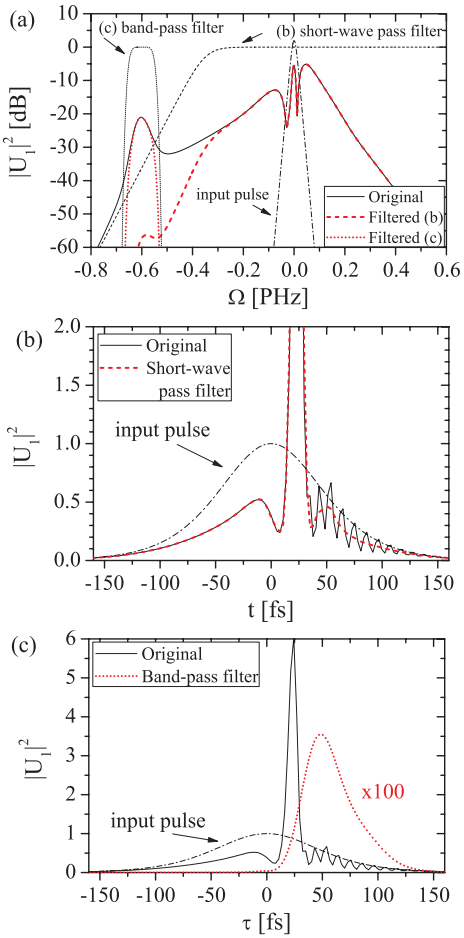

FIG. 5. (Color online) (a) shows the FW spectrum at the optimal compression point ($z = 38$ mm) for a simulation using the same parameters as the experiment in Ref. [7]: $\lambda_1 = 1.26\ \mu$m, $T_{\mathrm{in}}^{\mathrm{FWHM}} = 110$ fs, $I_{\mathrm{in}} = 35$ GW/cm^2, and $N_{\mathrm{eff}} = 4.1$. A dispersive wave is evident at $\Omega \simeq -0.6$ PHz ($\lambda = 2.11\ \mu$m). When a short-wave pass filter is applied (dashed), the trailing oscillations on the FW time trace can be filtered away; see (b). Instead when a bandpass filter is applied (dotted) centered at the dispersive wave peak, a clean 50 fs FWHM pulse with $\lambda = 2.11\ \mu$m results; see (c). The filtered radiation has for clarity been amplified 100 times; the peak intensity of this pulse is around 20 dB below the input peak intensity.

duration (around seven optical cycles and much shorter than the near-IR pump) and 120 nm FWHM bandwidth. These values give a time-bandwidth product around 30% above the transform limit. The efficiency of generating the Cherenkov radiation can be estimated by observing that the radiation intensity lies around 20 dB below the input level. A more precise value is obtained by integrating over the pulses, which reveals that around 1.5% of the input pulse energy flux resides in the dispersive wave. Considering that the 50 fs radiation is generated with a longer near-IR input pulse (110 fs FWHM), these numbers look quite favorable. A higher efficiency can be achieved shortly after the optimal compression point, as, e.g., evidenced by Fig. 3(c), where clearly the Cherenkov peak grows in strength after the soliton has been formed. For the case in Fig. 3(c) the efficiency is around 2% at the compression point and shortly after it increases to over 3%, after which it saturates.

IV. CHERENKOV RADIATION PHASE-MATCHING CURVES

In Fig. 6 we present the phase-matching curves (in absence of the nonlinear phase shift) for a broad range of nonlinear crystals previously used for cascaded quadratic interaction. We observe that the "low-dispersion" crystals (KDP, LBO) might generate near-IR dispersive waves when pumped at standard laser wavelengths for generating energetic femtosecond pulses ($\lambda = 0.8$–$1.3\ \mu$m), while BBO and the more dispersive crystals (LN, LT, KTP, KN, and KTA) when pumped with these wavelengths will generate dispersive waves in the mid-IR. In fact, the dispersive wave is in many cases phase matched

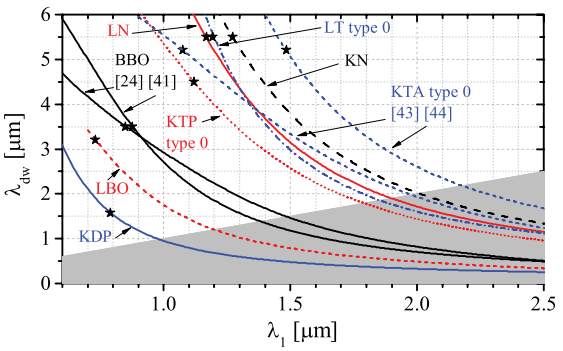

FIG. 6. (Color online) Phase-matching curves similar to Fig. 2 for various popular quadratic nonlinear crystals as calculated from Eq. (13) with $q_{sol} = 0$. The gray area denotes the regime with anomalous GVD for λ_1, where an effective self-focusing nonlinearity $n^I_{cubic} > 0$ is needed to generate solitons. The "0" transmission edge (through 1 cm of crystal) of the mid-IR absorption region is marked with a star. The phase matching considered is type I $oo \rightarrow e$, except where denoted "type 0," where $ee \rightarrow e$ interaction is considered. The KN and LN curves hold for both type-0 and type-I phase matching as they turn out to have almost identical phase-matching curves. The crystals are as follows (the Sellmeier equations are all taken at room temperature and are from Ref. [40], except where noted). KDP, potassium dihydrogen phosphate; LBO, lithium triborate; BBO, β–barium borate [24,41]; KTP, potassium titanyl phosphate; LT, lithium tantalate; LN, 5% magnesium oxide–doped lithium niobate [42]; KN, potassium niobate; KTA, potassium titanyl arsenate [43,44].

inside the absorption region of the crystal; the end of the mid-IR absorption region is marked with a star. In this case it is therefore not necessary to perform a postcompression filtering to avoid beating between the soliton and the dispersive wave; the filter is in a sense naturally built into the crystal. On the other hand, if the aim is to generate dispersive waves this diagram provides a quick overview of possible pump wavelengths and crystal candidates.

When pumped with Ti:sapphire lasers with $\lambda_1 \simeq 0.8\ \mu$m all the crystals shown in Fig. 6 have phase-matching points inside their respective IR absorption regions. This explains why dispersive waves have eluded observation despite the many experiments performed with this wavelength (e.g., [5,6]). Another explanation is, of course, that while many experiments have investigated cascaded SHG effects at this wavelength, the majority of these have been carried out far below the soliton formation threshold. Thus, a dispersive wave cannot form.

Note that these curves are based on the Sellmeier equations, which are usually only valid for a limited range; in particular, the mid-IR behavior of the Sellmeier equations has only recently been investigated for some crystals due to the current interest in mid-IR laser sources (BBO [24] and LN [42] are examples). Thus, the long-wavelength range of the calculations might not be very accurate for all crystals. In fact, we recently became aware of a new IR study on BBO [41], reporting on modified Sellmeier equations relative to those in Ref. [24]; this curve has been included in Fig. 6, and it is evident that the two predictions do not always agree. The same is the case for KTA, where two completely different curves are obtained.

V. EXPERIMENT

Recently, some of us investigated controllable self-steepening effects in cascaded SHG [21]. In preparing for this experiment a 25 mm BBO crystal cut with $\theta_c = 28^\circ$ was pumped at $\lambda_1 = 1.420\ \mu$m, close to the zero-dispersion point $\lambda_{ZD} \simeq 1.49\ \mu$m. The pulses were generated with an optical parametric amplifier and had a FWHM duration of 130 fs and 10 μJ energy. The input pulse spectrum was large enough to support an 89 fs FWHM pulse, corresponding to a dimensionless chirp parameter of around unity, and the pump pulse was loosely focused in the BBO crystal to generate an intensity in the tens of GW/cm^2 range. The loose focus (approximately 0.4 mm FWHM spot size) minimizes diffraction effects as the corresponding Rayleigh length is around ten times the crystal length.

A substantial spectral component was found to reside inside the linear region, i.e., beyond λ_{ZD}; see Fig. 7(a) where the linear region (with anomalous dispersion) is shaded gray. The position of the peak changed slightly when the phase-mismatch value was changed: for $\Delta k = 2.4\pi$/mm it is located around $\lambda = 1.65\ \mu$m, for $\Delta k = 4.0\pi$/mm it is located around $\lambda = 1.55\ \mu$m, while for $\Delta k = 5.8\pi$/mm it is located around the zero-dispersion point. Note that the spectrum analyzer in the experiment was not able to measure beyond $\lambda = 1.7\ \mu$m. This unpublished result is now investigated further so as to ascertain whether this is an observation of optical Cherenkov radiation.

Initially, we can say based on what we have presented so far in this paper that a dispersive wave should not change its spectral position when Δk is changed, but this is true

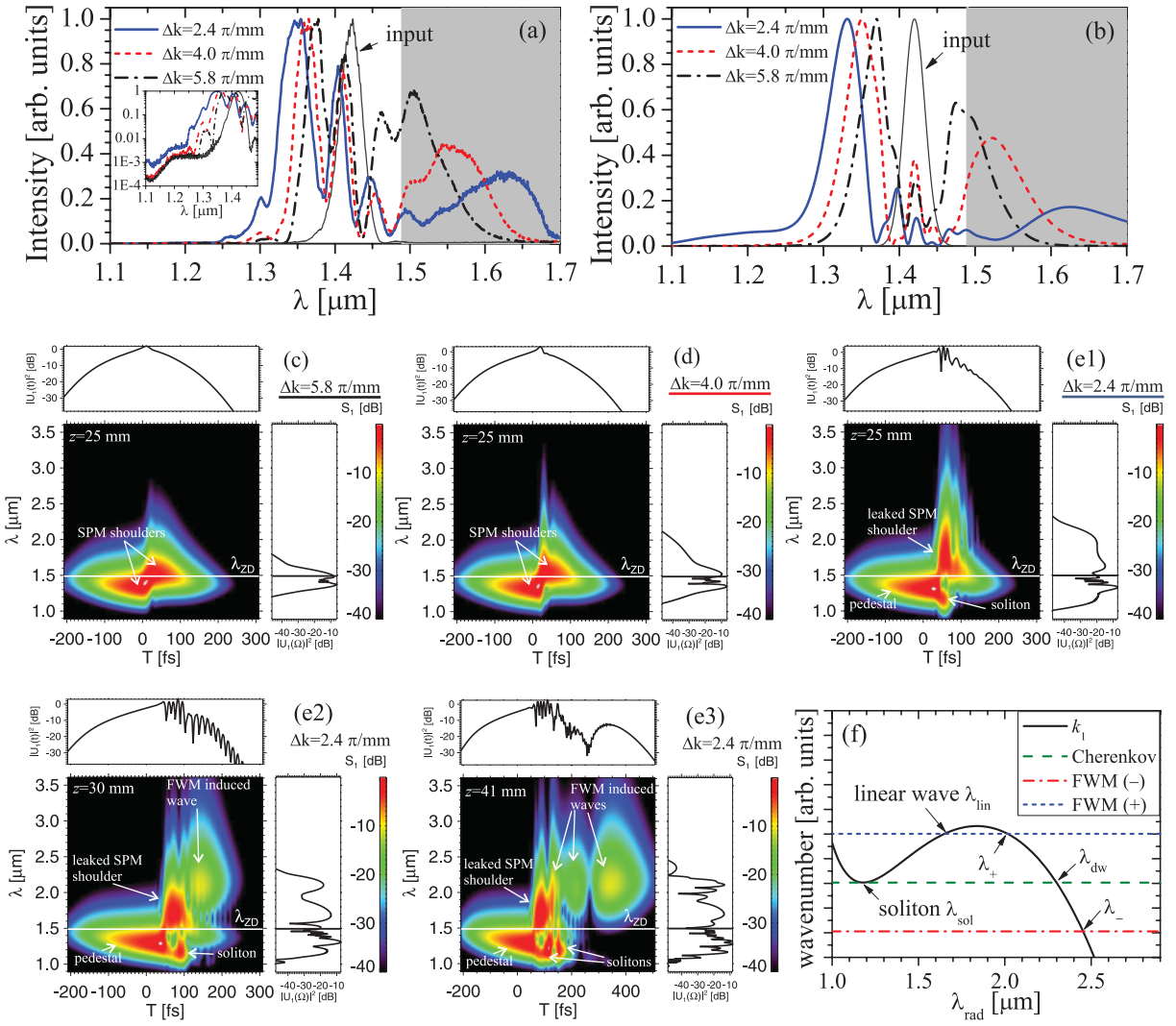

FIG. 7. (Color online) Experimental results (a) of a BBO crystal pumped close to λ_{ZD}, using a chirped $T_{in}^{FWHM} = 130$ fs pulse ($T_{in}^{FWHM} = 89$ fs transform limit) at $\lambda_1 = 1.420$ μm having 10 μJ of energy. The intensity was kept constant and the spectral trends are reported after 25 mm of propagation for $\Delta k = 5.8\pi/\text{mm}$, $\Delta k = 4.6\pi/\text{mm}$, and $\Delta k = 2.4\pi/\text{mm}$. The inset shows a zoom in the soliton region $\lambda = 1.1$–1.49 μm on a logarithmic scale. In (b) we show the result of numerical simulations after 25 mm of propagation. The input pulses were chirped Gaussian 130 fs FWHM pulses with $C = +1.0$. The same phase-mismatch values as in the experiments were used, and the intensities were $I_{in} = 70$ GW/cm^2 for $\Delta k = 5.8\pi/\text{mm}$ (giving $N_{eff} = 16.3$), $I_{in} = 55$ GW/cm^2 for $\Delta k = 4.6\pi/\text{mm}$ (giving $N_{eff} = 18.5$), and $I_{in} = 50$ GW/cm^2 for $\Delta k = 2.4\pi/\text{mm}$ (giving $N_{eff} = 24.0$). In both (a) and (b) the anomalous dispersion region is shaded gray. (c)–(e) Show the XFROG spectrograms of the FW taken with a 10 fs FWHM gating pulse; (e2) and (e3) show the case $\Delta k = 2.4\pi/\text{mm}$ at later stages. (f) Shows the calculations of FWM using Eq. (15) and using as input a soliton at $\lambda_{sol} = 1.18$ μm and a linear wave at $\lambda_{lin} = 1.65$ μm. The wave numbers shown have been compensated for the slope of the soliton group velocity.

only as long as the soliton does not change either its peak intensity substantially (so as to change q_{sol}) or if the soliton is strongly blue- or redshifted, whereby the phase-matching point may change quite dramatically. This cannot necessarily be confirmed for the experimental results in Fig. 7.

We have therefore performed numerical simulations using 130 fs FWHM chirped Gaussian input pulses (chirp parameter[4] $C = +1.0$). All parameters were the same as in the experiment, and the input intensity was varied in the $I_{in} = 50$–70 GW/cm^2 range to mimic the experimental spectra.[5] These intensities results in quite large soliton orders $N_{eff} > 10$.

In Fig. 7(b) we show on a linear scale the numerical spectra at $z = 25$ mm for each case. The general trend from the experiment is matched well, as a redshifted peak is observed in the linear regime and it is redshifted the most for low Δk

[4]The sign of the chirp is unknown, but a positive chirp from SPM in the beam path seems most likely. In any case, similar results were found with a negative chirp, although with a lower intensity.

[5]The experimental intensity fluctuations were probably lower than this, but instead the phase-mismatch values hold some degree of uncertainty justifying this approach.

values just as in the experiments. Also the blueshifted peaks match rather well with results of the experiments.

The XFROG spectrograms in Fig. 7 further explain the dynamics. Basically by decreasing the phase mismatch we increase the soliton order, and thereby the soliton compression point occurs sooner; thus what we see with a fixed crystal length, as in the experiment, is roughly the soliton compression dynamics at various stages.[6]

For $\Delta k = 5.8\pi/\text{mm}$, Fig. 7(c), the soliton order is too low for any soliton to form before the crystal exit after 25 mm of propagation; the spectrogram at $z = 25$ mm shows a strongly chirped pulse and clear SPM-like shoulders are visible in the spectral trace. Notice, however, how the redshifted shoulder has partially leaked into the anomalous dispersion region, $\lambda > \lambda_{ZD}$.

For $\Delta k = 4.0\pi/\text{mm}$, Fig. 7(d), we are now closer to the optimal compression point, and now the red SPM shoulder is actually pushed into the anomalous regime. This radiation gives rise to the strong peak in the nonsolitonic linear regime of the spectrum around $\lambda = 1.5$ μm and beyond.

For $\Delta k = 2.4\pi/\text{mm}$, Fig. 7(e1), Δk is decreased enough to obtain an effective soliton order high enough to form a soliton just before reaching $z = 25$ mm. In the spectrogram the soliton appears around $\lambda \simeq 1.20$ μm, i.e., strongly blueshifted, and ahead of the soliton an uncompressed part is located (the usual pedestal, located around $\lambda \simeq 1.30$ μm).

Therefore the main experimental peak in Fig. 7(a) to the blue side, which is gradually shifted toward shorter wavelengths when Δk is decreased, seems not to be solitonic radiation but instead is related to the uncompressed pedestal. Furthermore, the numerics confirm that this uncompressed pedestal is quite strong and that the soliton in the linear spectrum instead is almost unnoticeable: in Fig. 7(b) the soliton radiation is related to the broad low plateau centered around $\lambda = 1.20$ μm in the blue curve, while for the black and red curves no soliton is formed and the plateau is absent.

In order to determine whether the experiments show indications of such a plateau we have made an inset in Fig. 7(a) showing the short-wavelength range on a logarithmic scale. It seems that in the $2.4\pi/\text{mm}$ case the first signs of a plateau of radiation at $\lambda = 1.2$ μm are noticeable, suggesting the initial stage of the soliton formation seen in Fig. 7(e1).

Coming back to Fig. 7(e1), the SPM shoulder that has leaked into the anomalous regime temporally overlaps with the soliton and in the time trace trailing oscillations are seen on the pulse. Also some radiation is found around $\lambda \simeq 2.0$ μm. We now argue that this is not Cherenkov radiation, but rather radiation from four-wave mixing (FWM) of the soliton and the leaked SPM shoulder. Such a FWM between the soliton and a linear wave may generate new spectral components [28,45] in positions distinct from the dispersive wave phase-matching point. As mentioned previously the Cherenkov resonance condition can be written as $k_1(\omega_{dw}) = k_{sol}(\omega_{dw})$, while the two FWM resonance conditions from mixing the soliton and the linear wave are [28]

$$k_1(\omega_{rad}) = \pm[k_1(\omega_{lin}) - k_{sol}(\omega_{lin})] + k_{sol}(\omega_{rad}), \qquad (15)$$

where ω_{rad} is the radiative frequency of the wave resonant in this FWM.

In order to complete this argument we present the continuation of the simulation for $\Delta k = 2.4\pi/\text{mm}$ in Figs. 7(e2) and 7(e3). At $z = 30$ mm the soliton is now clearly separated from the pedestal (it is slowed down by the nonlocal effects that induce a Raman-like blueshift of the pulse to a regime with lower group velocity). The soliton peak is located around $\lambda = 1.18$ μm and due to their temporal overlap it may interact with the leaked SPM field in the anomalous regime (peaked around $\lambda = 1.65$ μm). At this point of propagation the peak around $\lambda = 2.10$ μm has grown to a substantial level. Calculations of the FWM phase-matching points from Eq. (15) presented in Fig. 7(f) show that it derives from FWM between the soliton and the leaked SPM field rather than Cherenkov radiation: the former is phase matched at $\lambda_+ \simeq 2.02$ μm, while the Cherenkov resonance is located around $\lambda_{dw} \simeq 2.3$ μm.

Upon further propagation to $z = 41$ mm, Fig. 7(e3), we can complete the picture: now the soliton fission process [16,39] has created two main solitons, and the different spectral peaks observed can be understood from FWM of these solitons with various parts of the radiation in the anomalous (linear) regime. In fact, we did not observe any Cherenkov radiation in the numerics, which could be because the pumping conditions were close to the zero-dispersion point, favoring the generalized FWM condition over the Cherenkov condition [46].

Concluding, we believe that the experimentally observed radiation peak in the linear regime is not optical Cherenkov radiation, but rather SPM-broadened radiation leaking into the linear regime. Nonetheless, through nonlinear FWM with the 1.2 μm soliton expected at longer propagation lengths, the experimentally observed leaked radiation peak should play an important role in the formation of new strongly redshifted Cherenkov-like waves.

This experimental and numerical investigation has therefore allowed us to identify an experimentally accessible set of conditions where highly redshifted radiation should be obtainable by a mechanism other than that of the Cherenkov radiation condition. This long-wavelength generation originates from nonlinear FWM dynamics between solitonic and leaked nonsolitonic radiation that naturally plays out during high-order soliton compression close to the zero-dispersion wavelength. Observation of the predicted long-wavelength peaks would require a spectrometer that goes beyond $\lambda = 1.7$ μm, and a more detailed investigation around and below $\lambda = 1.20$ μm, where the numerics predict the formation of the main soliton.

Finally, it is worth mentioning that the kind of dynamics discussed in this section—where the redshifted SPM shoulder leaks into the linear regime—was not observed in any of the simulations in Figs. 2–5, even when pumping very close to the zero-dispersion point. The explanation is that the soliton order was much lower there, so the amount of leaked SPM-broadened radiation was minimal. In fact, Fig. 8 compares the case in Fig. 7(e) pumped at $\lambda_1 = 1.42$ μm with a high

[6]Such reasoning holds only because the soliton orders in the three cases are quite similar.

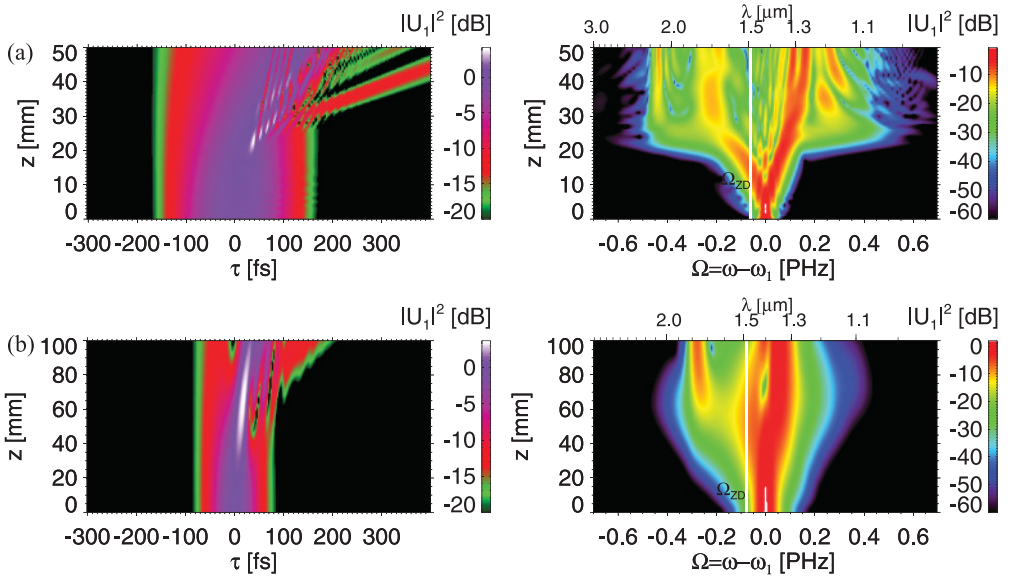

FIG. 8. (Color online) Comparing the evolution of the FW in the cases of (a) $\lambda_1 = 1.420$ μm used in Fig. 7 having $N_{\text{eff}} = 24.0$ and chirped input pulse ($T_{\text{in}}^{\text{FWHM}} = 130$ fs) and (b) $\lambda_1 = 1.400$ μm from Fig. 2 having $N_{\text{eff}} = 2.0$ and $T_{\text{in}}^{\text{FWHM}} = 50$ fs.

soliton order with a low-soliton case from Fig. 2 pumped at $\lambda_1 = 1.40$ μm. In contrast to the high-soliton-order case just studied, in the latter case there is only a small amount of leaked SPM-broadened radiation that later seems to be pulled back into the normal dispersion regime.

VI. CONCLUSIONS AND DISCUSSION

In this publication we have investigated the formation of optical Cherenkov radiation (dispersive waves) when generating solitons with ultrafast cascaded SHG of femtosecond pulses. Through numerical simulations of the full coupled propagation equations we showed the formation of dispersive waves in BBO for a broad range of FW wavelengths ($\lambda_1 =$ 0.95–1.45 μm). The dispersive wave formed in the linear part of the spectrum, i.e., the anomalous dispersion region, which is located in the red part of the spectrum. We explained the dispersive wave formation by reducing the coupled wave equations to a single NLSE-like equation for the FW. We calculated the phase-matching conditions analytically using the resonant coupling theory for the NLSE [12], and found good agreement with the numerical results.

Since the Cherenkov radiation often was formed very far from the soliton wavelength, we found it very important to describe the dispersion as accurately as possible. It is in this connection worth noting that dispersive waves require higher-order dispersion to exist: in fact the presence of third-order dispersion, i.e., the first higher-order contribution, tends to destabilize the otherwise stable soliton in the NLSE [2,11,12,47–49], and the soliton starts shedding radiation into the linear dispersive wave. Close to the zero-dispersion point λ_{ZD}, we may describe the system by TOD to a good approximation, but further away higher-order dispersion components become more crucial. Here we showed an example of such a system, where the soliton was generated far away from λ_{ZD}, and the spectral location of the dispersive waves therefore was shifted hundreds of nanometers when accurately describing the dispersion. This also explains why the dispersive wave in cascaded SHG has gone unnoticed so far (even if the numerical simulations in Ref. [7] indicate its presence), and also why we were unable to observe it with third-order dispersion alone in Ref. [10] when pumping a BBO crystal around 1.0 μm wavelength.

Optical Cherenkov radiation gives rise to a beating with the soliton that leads to ultrafast temporal oscillations in the trailing part of the compressed soliton. These oscillations can be removed after the compression by a suitably selected short-wave pass filter. On the other hand, we also showed that inserting a simple bandpass filter around the dispersive wave peak results in an ultrashort broadband mid-IR near-transform-limited pulse with a pulse duration much shorter than that of the near-IR pump and with a conversion efficiency around a few percent.

We also showed the phase-matching curves of a broad range of popular nonlinear crystals for cascaded interaction, and pointed out that the more dispersive crystals have phase-matching points to a dispersive wave quite far into the mid-IR spectrum, so that when pumped at standard laser wavelengths the crystal will automatically absorb the dispersive wave radiation.

In connection with a recent experiment published by some of us [21], an unexpected spectral peak was observed in the linear (anomalous dispersion) regime. We performed detailed numerical simulations to ascertain whether this could be the first observation of optical Cherenkov radiation in cascaded SHG. Based on simulations we concluded that for the parameters of the experiment the observed peak was not Cherenkov radiation. Instead, the peak could be explained by leaking of the red SPM shoulder into the linear regime: in the initial stages of propagation before soliton formation the cascaded SHG effectively induces a Kerr-like SPM action generating the characteristic spectrally broadened double shoulders in the FW spectrum. Being close to the zero-dispersion point, the red shoulder leaked into the linear regime. The fact that the peak

TABLE II. Simulation parameters used for Eq. (A1).

j	s_j	$\Delta\lambda_j$ (μm)	$\lambda_{0,j}$ (μm)	$n_{\mathrm{SG,j}}$
1	1.0	0.251	0.445	20
2	1.0	1.010	1.300	9
3	0.6	0.159	2.525	1
4	0.2	0.053	2.825	1
5	0.1	0.530	2.750	1

shifted toward longer wavelengths when the phase mismatch in the experiment was lowered was explained by a higher effective soliton order.

In the simulations performed to investigate the experimental results we did not observe clear signs of Cherenkov radiation, but we instead saw spectral peaks in the linear regime that we believe to be originating from four-wave mixing of the solitons and the leaked SPM shoulder. These peaks should be located slightly beyond the range of the spectrometer and were therefore not seen in the experiment, but the overall good agreement between the experiment and numerical simulations leads us to conclude that we have observed the precursors of the resonant peaks caused by mixing solitons and linear waves. We will pursue the observation of such spectral peaks in the future.

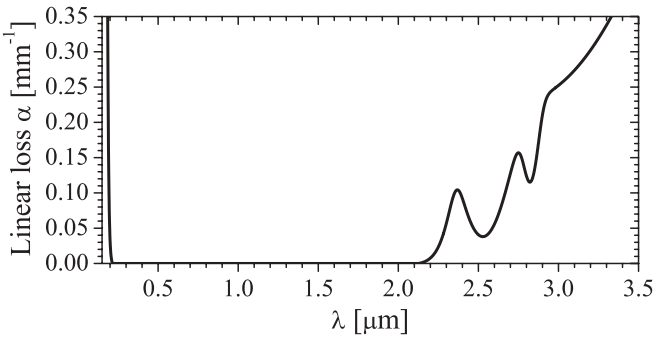

FIG. 9. The linear loss included in the simulation to simulate the absorption loss in BBO.

The observation of optical Cherenkov radiation in cascaded SHG of ultrafast femtosecond pulses underlines how many features this system has in common with soliton formation in optical fibers, and in particular with supercontinuum radiation. The advantage of the cascaded nonlinearity is as always that we have at hand a nonlinear system where the strength of the nonlinearity can be controlled continuously. Thus, investigation of dispersive waves in cascaded SHG might give insight into formation, control, and dynamics of the interaction, leading to improved sources for ultrashort pulses and broadband coherent light in the visible and mid-IR.

ACKNOWLEDGMENTS

Support is acknowledged from the Danish Council for Independent Research (Technology and Production Sciences, Grant No. 274-08-0479 "Femto-VINIR," and Natural Sciences, Grant No. 21-04-0506). Portions of this work were supported by the US National Science Foundation (Grant No. PHY-0653482). Michael Frosz is acknowledged for useful discussions.

APPENDIX A: MODELING THE UV AND IR LOSSES

An accurate numerical study of the mid-IR behavior of the Cherenkov radiation requires taking the losses in that region into account. In order to do this we used the approach mentioned in Ref. [50]: based on a typical transmission vs wavelength profile of BBO, as found, e.g., with the program SNLO [51], we constructed a transmission profile composed of five super-Gaussian functions,

$$T(\lambda) = \min\left\{ \sum_{j=1}^{5} s_j \exp\left[-\left(\frac{\lambda - \lambda_{0,j}}{\Delta\lambda_j} \right)^{2n_{\mathrm{SG,j}}} \right], 1 \right\}, \qquad \text{(A1)}$$

where the coefficients are listed in Table II. This was then converted to a wavelength-dependent linear loss coefficient α that was included in the simulations, and its profile is shown in Fig. 9: the short-wavelength UV edge is set to $\lambda = 0.189$ μm while the IR cutoff was $\lambda = 3.5$ μm [40], both defined by having $\alpha = 1$ mm^{-1}.

[1] P. A. Franken, A. E. Hill, C. W. Peters, and G. Weinreich, Phys. Rev. Lett. **7**, 118 (1961).
[2] P. K. A. Wai, C. R. Menyuk, Y. C. Lee, and H. H. Chen, Opt. Lett. **11**, 464 (1986).
[3] R. DeSalvo, D. Hagan, M. Sheik-Bahae, G. Stegeman, E. W. Van Stryland, and H. Vanherzeele, Opt. Lett. **17**, 28 (1992).
[4] A. V. Buryak, P. Di Trapani, D. V. Skryabin, and S. Trillo, Phys. Rep. **370**, 63 (2002).
[5] X. Liu, L. Qian, and F. W. Wise, Opt. Lett. **24**, 1777 (1999).
[6] S. Ashihara, J. Nishina, T. Shimura, and K. Kuroda, J. Opt. Soc. Am. B **19**, 2505 (2002).
[7] J. Moses and F. W. Wise, Opt. Lett. **31**, 1881 (2006).
[8] L. Bergé, O. Bang, J. J. Rasmussen, and V. K. Mezentsev, Phys. Rev. E **55**, 3555 (1997).
[9] M. Nisoli, S. D. Silvestri, and O. Svelto, Appl. Phys. Lett. **68**, 2793 (1996).
[10] M. Bache, O. Bang, W. Krolikowski, J. Moses, and F. W. Wise, Opt. Express **16**, 3273 (2008).
[11] P. K. A. Wai, H. H. Chen, and Y. C. Lee, Phys. Rev. A **41**, 426 (1990).
[12] N. Akhmediev and M. Karlsson, Phys. Rev. A **51**, 2602 (1995).
[13] F. W. Wise, I. A. Walmsley, and C. L. Tang, Opt. Lett. **13**, 129 (1988).
[14] A. S. Gouveia-Neto, M. E. Faldon, and J. R. Taylor, Opt. Lett. **13**, 770 (1988).
[15] S. Kelly, Electron. Lett. **28**, 806 (1992).
[16] A. V. Husakou and J. Herrmann, Phys. Rev. Lett. **87**, 203901 (2001).

[17] J. Herrmann, U. Griebner, N. Zhavoronkov, A. Husakou, D. Nickel, J. C. Knight, W. J. Wadsworth, P. S. J. Russell, and G. Korn, Phys. Rev. Lett. **88**, 173901 (2002).
[18] J. M. Dudley, G. Genty, and S. Coen, Rev. Mod. Phys. **78**, 1135 (2006).
[19] G. Krauss, S. Lohss, T. Hanke, A. Sell, S. Eggert, R. Huber, and A. Leitenstorfer, Nature Photon. **4**, 33 (2010).
[20] G. Chang, L.-J. Chen, and F. X. Kärtner, Opt. Lett. **35**, 2361 (2010).
[21] J. Moses and F. W. Wise, Phys. Rev. Lett. **97**, 073903 (2006); see also e-print arXiv:physics/0604170.
[22] C. R. Menyuk, R. Schiek, and L. Torner, J. Opt. Soc. Am. B **11**, 2434 (1994).
[23] M. Bache, J. Moses, and F. W. Wise, J. Opt. Soc. Am. B **24**, 2752 (2007).
[24] D. Zhang, Y. Kong, and J. Zhang, Opt. Commun. **184**, 485 (2000).
[25] M. Bache, O. Bang, J. Moses, and F. W. Wise, Opt. Lett. **32**, 2490 (2007).
[26] M. Bache and F. W. Wise, Phys. Rev. A **81**, 053815 (2010).
[27] F. Ö. Ilday, K. Beckwitt, Y.-F. Chen, H. Lim, and F. W. Wise, J. Opt. Soc. Am. B **21**, 376 (2004).
[28] A. V. Yulin, D. V. Skryabin, and P. S. J. Russell, Opt. Lett. **29**, 2411 (2004).
[29] A. L. Gaeta, Opt. Lett. **27**, 924 (2002).
[30] J. M. Harbold, F. Ö. Ilday, F. W. Wise, T. A. Birks, W. J. Wadsworth, and Z. Chen, Opt. Lett. **27**, 1558 (2002).
[31] D. V. Skryabin, F. Luan, J. C. Knight, and P. S. J. Russell, Science **301**, 1705 (2003).
[32] P. Falk, M. H. Frosz, O. Bang, L. Thrane, P. E. Andersen, A. O. Bjarklev, K. P. Hansen, and J. Broeng, Opt. Lett. **33**, 621 (2008).
[33] I. Cristiani, R. Tediosi, L. Tartara, and V. Degiorgio, Opt. Express **12**, 124 (2003).
[34] A. V. Gorbach and D. V. Skryabin, Phys. Rev. A **76**, 053803 (2007).
[35] A. V. Gorbach and D. V. Skryabin, Nature Photon. **1**, 653 (2007).
[36] I. Kang, S. Smolorz, T. Krauss, F. Wise, B. G. Aitken, and N. F. Borrelli, Phys. Rev. B **54**, R12641 (1996).
[37] M. Bache, B. B. Zhou, and F. W. Wise (unpublished).
[38] J. N. Elgin, T. Brabec, and S. M. J. Kelly, Opt. Commun. **114**, 321 (1995).
[39] Y. Kodama and A. Hasegawa, IEEE J. Quantum Electron. **QE-23**, 510 (1987).
[40] D. Nikogosyan, *Nonlinear Optical Crystals: A Complete Survey* (Springer, Berlin, 2005).
[41] K. Kato, N. Umemura, and T. Mikami, Proc. SPIE **7582**, 75821L (2010) [http://link.aip.org/link/?PSI/7582/75821L/1].
[42] O. Gayer, Z. Sacks, E. Galun, and A. Arie, Appl. Phys. B **91**, 343 (2008).
[43] J.-P. Fève, B. Boulanger, O. Pacaud, I. Rousseau, B. Ménaert, G. Marnier, P. Villeval, C. Bonnin, G. M. Loiacono, and D. N. Loiacono, J. Opt. Soc. Am. B **17**, 775 (2000).
[44] K. Fradkin-Kashi, A. Arie, P. Urenski, and G. Rosenman, Opt. Lett. **25**, 743 (2000).
[45] D. V. Skryabin and A. V. Yulin, Phys. Rev. E **72**, 016619 (2005).
[46] A. V. Gorbach, D. V. Skryabin, J. M. Stone, and J. C. Knight, Opt. Express **14**, 9854 (2006).
[47] V. I. Karpman, Phys. Rev. E **47**, 2073 (1993).
[48] J. N. Elgin, Opt. Lett. **17**, 1409 (1992).
[49] J. N. Elgin, Phys. Rev. A **47**, 4331 (1993).
[50] M. Bache, J. Opt. Soc. Am. B **26**, 460 (2009).
[51] [http://www.as-photonics.com/SNLO.html].